Chemical Engineering Journal 394 (2020) 124822

Contents lists available at ScienceDirect

Chemical Engineering Journal

journal homepage: www.elsevier.com/locate/cej

Supramolecular preorganization effect to access single cobalt sites for enhanced photocatalytic hydrogen evolution and nitrogen fixation

Wenyao Zhang[a,b], Yongsheng Fu[a,*], Qiong Peng[a], Qiushi Yao[c], Xin Wang[a], Aiping Yu[b,*], Zhongwei Chen[b,*]

[a] Key Laboratory of Soft Chemistry and Functional Materials, Nanjing University of Science and Technology, Ministry of Education, Nanjing 210094, China
[b] Waterloo Institute for Nanotechnology, University of Waterloo, Waterloo, Ontario N2L3G1, Canada
[c] Department of Physics, Southern University of Science and Technology, Shenzhen 518055, China

HIGHLIGHTS

- A supramolecular anchoring strategy is reported to stabilize single-atom-dispersed cobalt.
- The Co@g-C_3N_4 possess a negative Fermi level & a high energy level of *d*-band position.
- Single-site Co atom facilitates the activation of N_2 on the surface of g-C_3N_4.
- Single-site Co atom accelerates the interfacial charge transfer process on g-C_3N_4.
- The Co@g-C_3N_4 shows improved photocatalytic H_2 evolution and N_2 fixation performances.

GRAPHICAL ABSTRACT

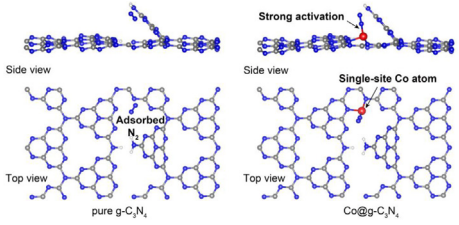

ARTICLE INFO

Keywords:
Single-atom catalyst
Supramolecular
Graphitic carbon nitride
Synergistic active centers
Photocatalytic hydrogen evolution
Photocatalytic nitrogen fixation

ABSTRACT

Ever-increased investigation has been focused on designing photocatalysts comprising intimately interfaced photo-absorbers and co-catalysts for promoting the separation of electron-hole pairs and surface redox reaction. Herein, we present a photocatalytic system in which the single-site-cobalt-atom is firmly trapped and stabilized into the frameworks of porous crimped graphitic carbon nitride (g-C_3N_4), proposing as advanced photocatalysts for solar-photon-driven hydrogen production and nitrogen fixation. A single molecular source of dicyandiamide was used to partly transformed and then *in-situ* preorganized into supermolecular precursor, which could coordinate with cobalt ions and manipulate the interactions under elevated temperature prior to the condensation to form atomically Co dispersed g-C_3N_4 materials. Theoretical evaluation and experimental validation identified that the chemical integration of single-site-cobalt-atom on g-C_3N_4 is critical in optimizing the electron and band structures and accelerating the interfacial charge transfer process. As a result, the as-obtained Co@g-C_3N_4 possesses an exceptional photocatalytic hydrogen production rate (2481 $\mu molh^{-1}g^{-1}$, $\lambda > 420$ nm) and conspicuous nitrogen photofixation performances under visible-light irradiation. Such concerted catalysis attributes to the negative shift of the Fermi level in Co@g-C_3N_4 system deriving from the induced charge-transfer effect, which effectively gains the reducibility of electrons and creates more active sites for photocatalytic reactions.

* Corresponding authors.
E-mail addresses: fuyongsheng@njust.edu.cn (Y. Fu), aipingyu@uwaterloo.ca (A. Yu), zhwchen@uwaterloo.ca (Z. Chen).

https://doi.org/10.1016/j.cej.2020.124822
Received 27 December 2019; Received in revised form 12 March 2020; Accepted 19 March 2020
Available online 20 March 2020
1385-8947/

1. Introduction

Ever since the photoelectric effects were reported by the French scientist of Edmond Becquerel [1], scientific researchers become being addicted to engineering artificial photosynthetic systems to efficiently convert solar energy into chemical fuels on a scale. Photocatalytic hydrogen production and nitrogen fixation gradually stand out owing to the fact that hydrogen and ammonia are considered as the leading chemical molecules for meeting the demands of developing a clean, sustainability and carbon-neutral society [2]. Semiconductor materials, at the heart of either system, are theoretically considered to harvest solar energy and transform absorbed solar photons to the excited electron-hole pairs for driving the photocatalytic reactions including splitting water into hydrogen [3] and converting nitrogen to ammonia [2]. Thus seeking for an efficient semiconductor photocatalyst is the main key to offering the above promise but it still faces several challenges. Desired photocatalysts should fulfill stringent requirements such as (i) moderate bandgap for harvesting wide range of sunlight, (ii) suitable band levels for energy conversion, and (iii) highly prominent charge separation and transfer under illumination.

Graphitic carbon nitride (g-C_3N_4) is proposed as one of the outstanding candidates for such photocatalysts, which can challenge the kinetically sluggish multi-electron reactions due to its suitable band levels, tunable molecular properties, and excellent stability under harsh conditions [3,4]. After intensive investigations, it is found that the optical properties of g-C_3N_4-based materials are thoroughly dependent on their morphologies, structural defects, surface areas, and energy states along with their electronic properties [5,6]. In this context, plenty of functionalization and modification synthesis methods have been developed for narrowing their bandgap for catching more visible photons, engineering their band structures, as well as optimizing their HOMO-LUMO energy levels. The details include the exfoliation of bulk g-C_3N_4 into two-dimensional g-C_3N_4 nanosheets to increase its specific surface areas [7,8], the use of a template to introduce porous structure [9–11], copolymerization with other polymers [12], the incorporation of new heteroatoms to manipulate g-C_3N_4′s electronic, optical and catalytic properties [13–17], et al. Among them, supramolecular chemistry approach is considered as one of the most efficient ways to modify the electron and band structures of g-C_3N_4 and meanwhile favors fabricating ordered structures including spheres, hollow spheres, hexagonal prism assemblies, nanotubes, and ultrathin 2D nanosheets [5,18]. In addition, the supramolecular approach associates the non-covalent interactions like hydrogen bonding to directly assemble into ordered stable aggregates under equilibrium conditions. One typical supramolecular structure is cyanuric acid-melamine (CM) complex which is joined by intermolecular hydrogen bonds. This CM complex is constructed by the hydrogen bonds of N-H···N and N-H···O with a molar ratio of 1:1, and could form various morphologies lying on their aligning and precipitating solvents. Obviously, water is the most common solvent for adopting the form of a stable hydrogen-bonded supramolecular. It is worth noting that melamine can be transformed into cyanuric acid molecule under a specific pH value [19]. Inspired by this point, constructing the supramolecular precursors for achieving tunable electronic/band structural g-C_3N_4 only from a single molecular source is highly desired recently.

On the other hand, to competently realize the solar-photon-driven hydrogen production and nitrogen fixation, either enhancing charge separation and transportation efficiency or promoting the surface reaction kinetics also needs to be improved to a great extent in practical. Especially, constructing heterojunctions has been proved to be an effective and efficient pathway, and hence numerous attempts have been reported [20]. For instance, incorporating metal (Fe, Cu, Ni) species into the intrinsic structure of g-C_3N_4 at an isolated single-site modality is able to enormously enhance the photocatalytic activities due to both the modification of the electronic/band structures and the facilitation of the interfacial charge transfer process [21–25]. Importantly, the high levels of pyridine-like nitrogen and the periodic cavities in g-C_3N_4 makes it an ideal host to firmly trap and stabilize the single-site metal cocatalysts. The unpaired electrons on pyridine-like nitrogen atoms could sufficiently capture the metal ions [26], and simultaneously the homogeneous periodic neighboring nitrogen could serve as coordinators and favorably progress the coordination reactions between the metal and g-C_3N_4. The robust metal-nitrogen interactions, in turn, impedes the dissolution, migration, and aggregation of the metal atoms, which identically provides abundant precise information toward the identification of catalytically active sites [27,28]. However, exhaustive understanding of the methods of metal introduction and the types and amounts of metal incorporation remains a great challenge for design and developing the single-atom modified heterophotocatalysts.

In this work, we report a molecular scaffolding strategy for directly trapping and stabilizing single-site cobalt in the frameworks of porous crimped graphitic carbon nitride (Co@g-C_3N_4), proposing as high-performance photocatalysts in solar-photon-driven hydrogen production and nitrogen fixation. A single molecular source of dicyandiamide was used to be partly transformed into dicyandiamidine nitrate under the assistance of nitrate acid, and then in situ construct a crimped supramolecular precursor through the intermolecular self-assembly behaviour between dicyandiamide and dicyandiamidine nitrate. After the introduction of cobalt chloride and the following thermal treatment process, the precursor was converted to g-C_3N_4 via a series of complicated polycondensation reactions while the well-coordinated cobalt ions were reduced and atomically embedded in the g-C_3N_4 matrix. Experimental investigation and density functional theory (DFT) computation strongly confirmed that an optimized electronic band structure of the resulting Co@g-C_3N_4 with a narrowed bandgap, an appropriate d-band position as well as suitable LUMO energy level can be obtained significantly. This Co@g-C_3N_4 shows much greatly enhanced solar-photon-driven activities including, exceptional photocatalytic hydrogen production rate (2481 μmol h^{-1} g^{-1}, $\lambda > 420$ nm) and conspicuous nitrogen photofixation under visible-light illumination.

2. Results and discussion

The detailed crystal and chemical structures of the supramolecular precursor were first characterized by powder X-ray diffraction pattern (XRD), Fourier-transform infrared spectroscopy (FT-IR), and scanning electron microscopy (SEM). Evidence of the formation of supramolecular is provided by FT-IR spectroscopy and XRD analysis (Fig. S1). The disappearance of C≡N absorption peaks and the formation of the stretching vibration of the C═O group in the FT-IR spectra sufficiently confirm the hydrolysis of dicyandiamide to dicyandiamidine nitride, as illustrated in Fig. 1a (i). Additionally, arising up of the stretching vibrations of O—H group attributes to the construction of the hydrogen bonds between dicyandiamide and dicyandiamidine nitrate (reaction (ii) in Fig. 1a), which plays a critical role in fabricating the supramolecular structures [18,29]. XRD patterns clearly demonstrated the additional new peaks in comparison with the starting dicyandiamide, giving a strong proof of the creation of new arrangements [21]. This phenomenon is further completely confirmed by the SEM images in Fig. S2, where a well-defined porous crimped morphology of the supramolecular precursor was observed significantly. On the other hand, after introducing cobalt ions, the lone pair electrons in dicyandiamidine nitrate could provide a strong coordinate environment for anchoring and stabilizing the cobalt ions, forming a stable complex, as described in reaction (iii) in Fig. 1a [46].

In order to create photoactive g-C_3N_4-based catalysts, the supramolecular precursor and cobalt ion coordinated supramolecular was then thermally treated at 550 °C under N_2 atmosphere. Fig. S3a exhibits the typical XRD patterns of pure g-C_3N_4 and Co@ g-C_3N_4 with various cobalt contents. The diffraction peak around 27.7° that signifies the characteristic signal of interlayer stacking can be noticed for pure g-C_3N_4, while the ones for Co@g-C_3N_4 is slightly shifted toward higher

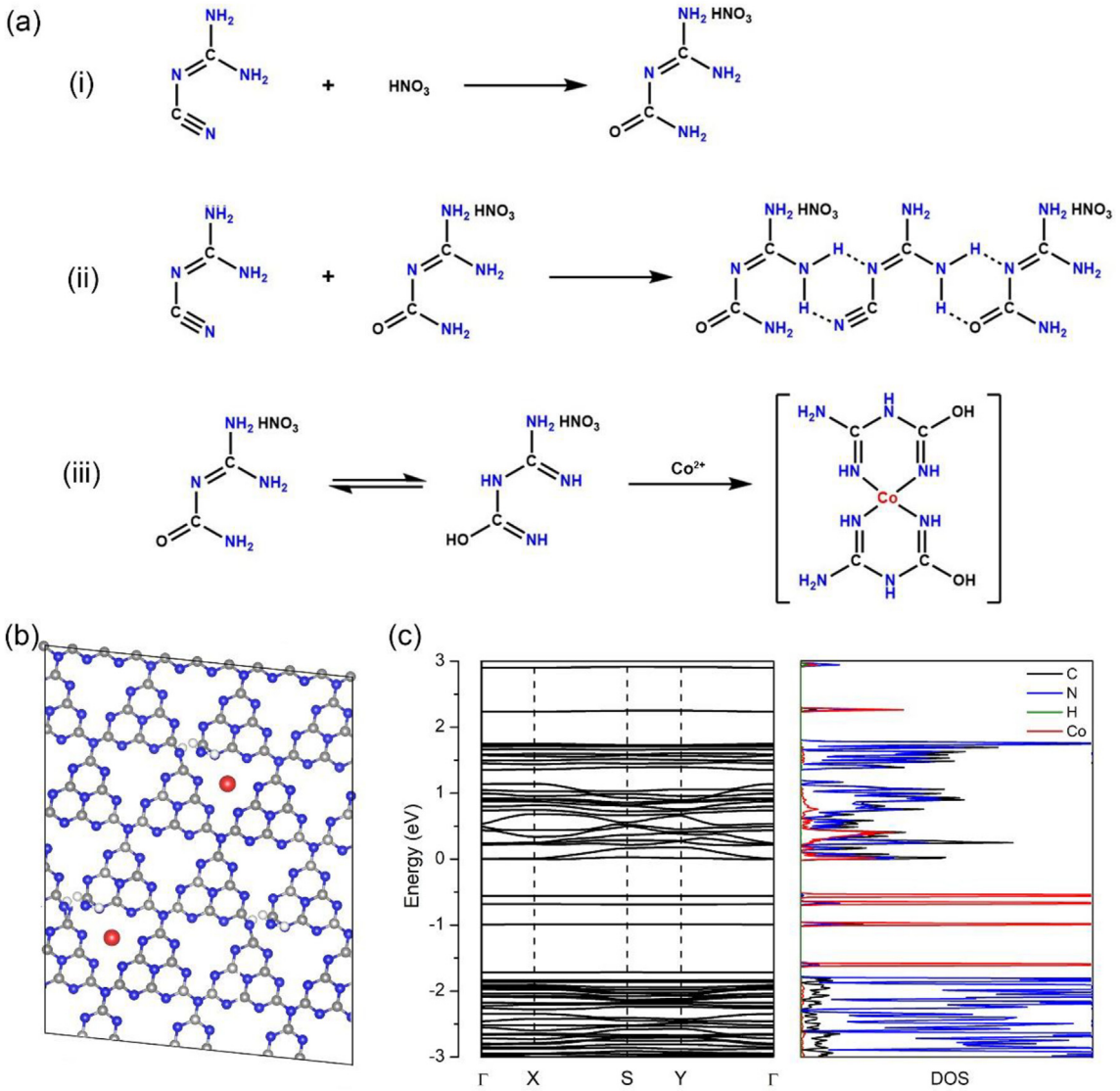

Fig. 1. (a) Proposed reaction process for forming the Co@g-C_3N_4 catalyst. (b) Proposed Co@g-C_3N_4 structure and (c) DFT calculated electronic properties of the Co@g-C_3N_4. The red, blue, gray, and white spheres denote Co, N, C, and H atoms, respectively. (For interpretation of the references to colour in this figure legend, the reader is referred to the web version of this article.)

angle and becomes less pronounced and broader upon the increase in cobalt. It should be noted that there is no signal associating with cobalt species including cobalt, cobalt chlorides, cobalt nitrides, cobalt carbides, and cobalt oxides, which is strongly demonstrated that cobalt ions are effectively embedded in the intrinsic structures of g-C_3N_4. FT-IR spectra in Fig. S3b reveals that the characteristic peak at 810 cm^{-1} and those in the range of 1200 ~ 1600 cm^{-1} deriving from the breathing vibration mode of tri-s-triazine subunits [21] and the collective wagging modes of the N and C atoms can be detected among all of the Co@g-C_3N_4 samples. This indicates that the cobalt was embedded into the structural cavities of g-C_3N_4 without breaking their original graphitic C-N network.

To further understand the electronic structures of the single-site Co atom embedded g-C_3N_4 composite, DFT computation was first conducted. Fig. 1b shows the proposed geometry structure of Co@g-C_3N_4. We theoretically evaluated the bandgap of this Co@g-C_3N_4 semiconductor. Although it may be a little underestimated [30,31], the Co@g-C_3N_4 shows a remarkably reduced bandgap, a flat band structure, and suitable LUMO energy levels for both hydrogen evolution and nitrogen fixation, Notably, the reduced bandgap structures of Co@g-C_3N_4 could significantly enhance the visible light-harvesting ability. Further examination of the *d*-band center based on the PDOS analyses was figured subsequently (Fig. 1c and Fig. S4), determining that of −1.41 eV for Co@g-C_3N_4. Such a high d-band position leads to a closer *d*-center to the Fermi level, which is of electronic origin, therefore leads to a relatively enhanced reactivity.

Then we selected the Co@g-C_3N_4-1 composite, obtained by pyrolysis of 1 mg cobalt chloride with 2 g supramolecular precursor, as a representative model to investigate their morphology and chemical composition in detail. As shown in Fig. S5 and Fig. 2a, it's obvious that our pre-supramolecular synthesis could significantly result in a porous crimped sheets morphology in the final material, which makes the resultant g-C_3N_4 possess a large specific surface area of 33.7 $m^2\ g^{-1}$ and the Co@g-C_3N_4-1 possess that of 65.7 $m^2\ g^{-1}$, much more competitive than bulk g-C_3N_4 (13.2 $m^2\ g^{-1}$) only using dicyandiamide as the precursor (Fig. S6, Table S1). Moreover, the TEM image in Fig. 2b undoubtedly evident that the Co@g-C_3N_4-1 is entirely composed of uniform ultrathin nanosheets, and the presence of wrinkles reveals good flexibility of the sample. No clusters or nanoparticles can be found and the dominance of individual Co atoms on g-C_3N_4 was directly verified by atomic resolution high-angle annular dark-field scanning transmission electron microscopy (HAADF-STEM). Homogeneously dispersed

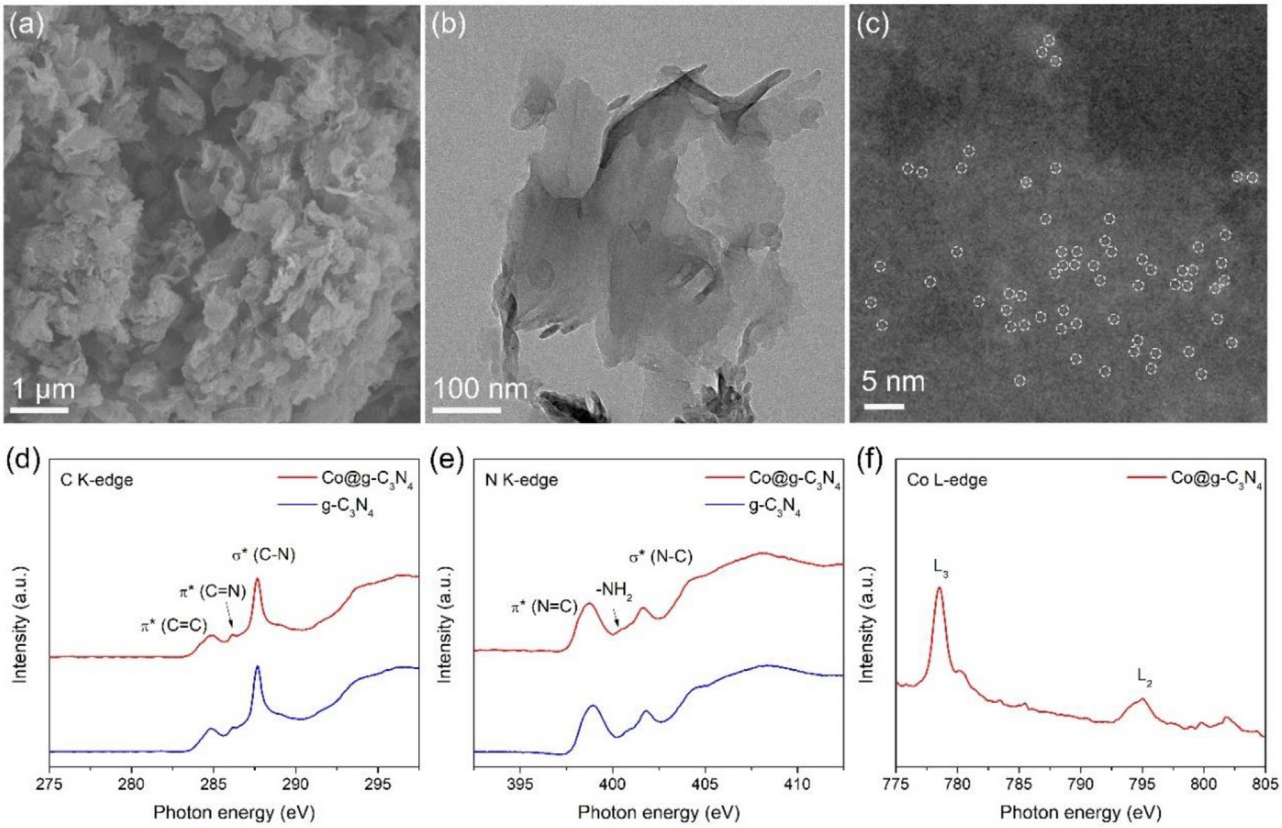

Fig. 2. (a) Typical SEM image, (b) TEM image, (c) HAADF-STEM of the Co@g-C_3N_4 composite, (d) C K-edge, (e) N K-edge and (f) Co L-edge XANES of the Co@g-C_3N_4 composite and pure g-C_3N_4.

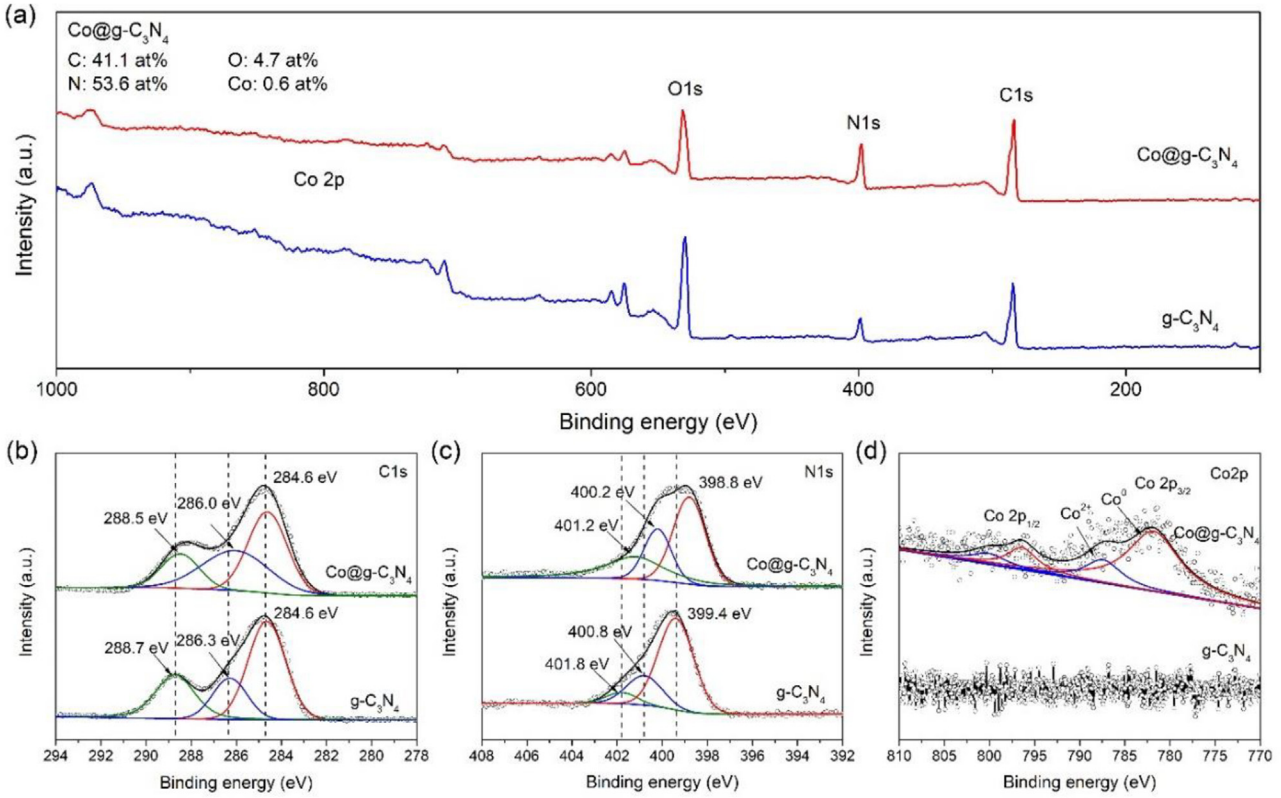

Fig. 3. XPS analysis of the Co@g-C_3N_4 composites. (a) The XPS survey spectrum of Co@g-C_3N_4 and pure g-C_3N_4. High-resolution (b) C 1s, (c) N 1s and (d) Co 2p XPS spectra of Co@g-C_3N_4 and pure g-C_3N_4, respectively.

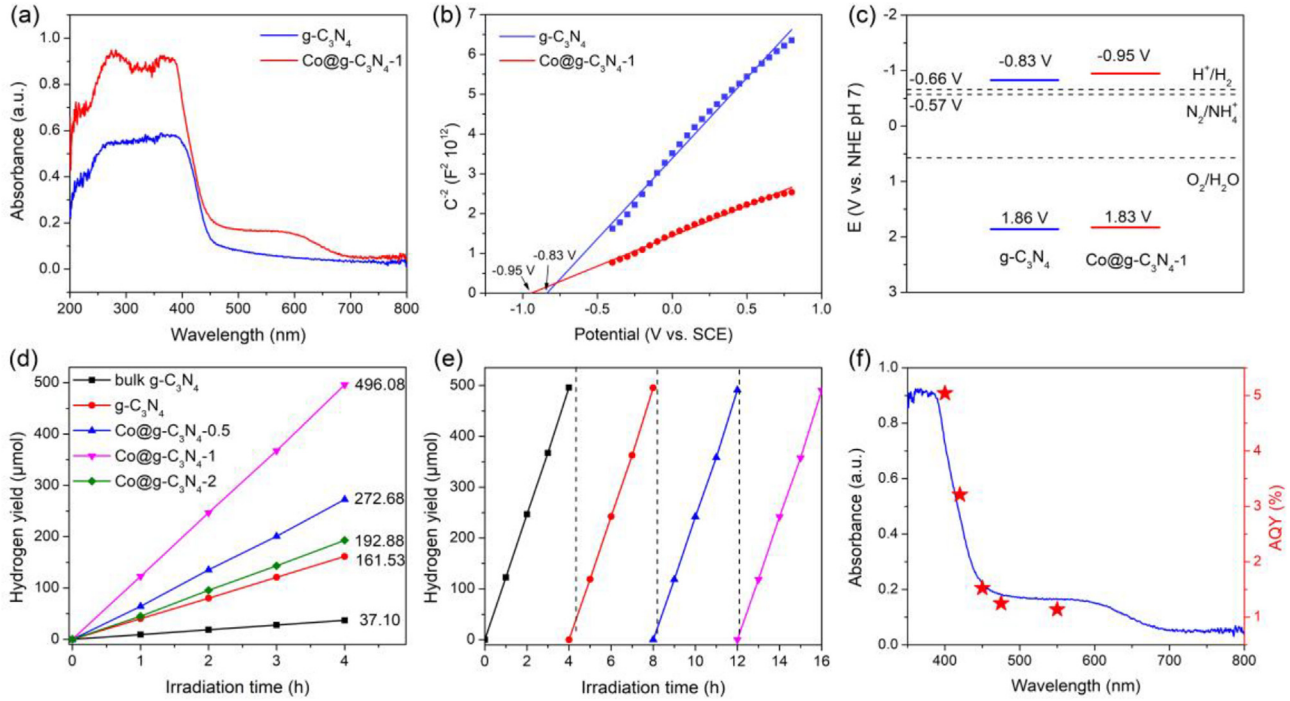

Fig. 4. (a) UV–vis absorbance spectra of pure g-C_3N_4 and Co@g-C_3N_4-1, (b) Mott-Schottky plots of pure g-C_3N_4 and Co@g-C_3N_4-1, (c) band structure of pure g-C_3N_4 and Co@g-C_3N_4-1 determined by UV–vis and Mott-Schottky analysis, (d) Time course of H_2 production from water with different catalysts under visible light irradiation; (e) cycling measurements of H_2 generation of Co@g-C_3N_4-1, (f) Wavelength dependent apparent quantum yield (AQY) of H_2 evolution over Co@g-C_3N_4-1 (right axis) and UV–vis light absorption spectra (left axis).

atomic Co sites (marked with white circles) were clearly observed throughout the carbon nitride nanosheet (Fig. 2c). A distinguishable cobalt signal can be detected in the corresponding energy dispersive X-ray (EDX) spectrum, proving again the successful incorporation of cobalt, and the EDX elemental mapping analysis demonstrates that the signals of Co, C, and N are completely superimposed on each other, at least on the nanoscale, suggesting that Co might be boned with C or N (Fig. S7).

To unravel the chemical states and coordination environment in Co@g-C_3N_4-1, we performed Synchrotron-based X-ray absorption fine structure spectroscopy analysis. In the C K-edge spectra (Fig. 2d), both the pure g-C_3N_4 and Co@g-C_3N_4-1 shows characteristic resonances of carbon nitride materials including the π* (C═C) at 284.9 eV, π* (C═N) at 286.1 eV, σ* (C−N) at 287.6 eV, as well as the typical pyridinic-like structure at ~293 eV.[21] In N K-edge spectra (Fig. 2e), two typical π* resonances at 398.7 eV and 401.5 eV correspond to the pyridinic-nitrogen in tri-s-triazine heterorings and the graphitic-nitrogen bridging among tri-s-triazine subunits, respectively. In addition, a weak signal located at 400.9 eV ascribes to the resonance of edge-site amino groups (−NH_2). With respect to the pure g-C_3N_4, the Co@g-C_3N_4-1 presents an evident decrease in the number of C-N bonds, as a result of the structural defects deriving from the introduction of Co-N coordinate covalent bonds. Furthermore, the Co L-edge spectrum of Co@g-C_3N_4-1 exhibits two broad multiple structures of L2 and L3 edges, that are separated due to the spin-orbit coupling effect. Upon detailed analysis, it is suggested the valence of Co species in Co@g-C_3N_4-1 was situated between Co (II) and Co(III), manifesting the ionic $Co^{\alpha+}$ ($+3 > \alpha > +2$) nature in the single-site Co@g-C_3N_4-1 composite, which coincides well with the reported results of the valence states of isolated single-site Co catalysts [32–34].

The detailed composition information of the Co@g-C_3N_4-1 architecture was further analyzed by X-ray photoelectron spectroscopy (XPS). Fig. 3a illustrates the XPS survey spectra of pure g-C_3N_4 and Co@g-C_3N_4-1, and that of Co@g-C_3N_4-1 reveals typical C1s, N1s, O1s, and Co 2p signals without any other impurities, in accordance with the above-mentioned elemental mapping analysis and EDX results. Moreover, the contents of C, N, O, and Co are determined to be 41.1, 53.6, 4.7 and 0.6 at%, respectively. The complex C1s spectrum exhibited in Fig. 3b was deconvoluted into three main peaks at the binding energy of 284.6, 286.3 and 288.5 eV, corresponding to the sp^2 C−C, sp^2 C−N, and sp^3 C−N groups, respectively. A summary of C 1s XPS analysis for Co@g-C_3N_4-1 and pure g-C_3N_4 samples was listed in Table S2. It can be clearly seen that the percentage of sp^3 C−N in Co@g-C_3N_4-1 is 18.17%, which is reduced compared with that of pure g-C_3N_4 of 19.04%, agreeing well with the XANES analysis in Fig. 2d. Additionally, in the N1s XPS spectra in Fig. 3c, for pure g-C_3N_4, three types of nitrogen components including graphitic N at 401.2 eV, pyrrolic N at 400.2 eV, and pyridinic N at 398.8 eV can be certainly identified, which are the characteristic nitrogen frameworks for g-C_3N_4 materials. Compared with pure g-C_3N_4, an evident change has been examined that all of these nitrogen components in Co@g-C_3N_4-1 shifted toward low binding energies. Such a phenomenon is caused by the strong interactions between Co and g-C_3N_4 support, where the nitrogen in tri-s-triazine heterorings would donate unpaired electrons to their neighboring cobalt possessing strong electron capture abilities. That is, the charge transfer process spontaneously occurs to optimize the delocalized conjugated π-electrons, leading to an optimized electronic/band structure of Co@g-C_3N_4-1, which is well consistent with the DFT computation results in Fig. 1. For Co 2p XPS spectrum in Fig. 3d, the binding energy of the Co $2p_{3/2}$ peak is 781.9 eV, which is considered as the characteristics for the Co^{2+} species, further confirming the Co atoms are strongly coordinated in the structure of g-C_3N_4.

After that, the optical properties and band structures of the Co@g-C_3N_4-1 compared to pure g-C_3N_4 were investigated via UV–vis absorbance spectra and Mott-Schottky analysis. It is clear that either pure g-C_3N_4 or Co@g-C_3N_4-1 possesses a typical semiconductor absorption behavior shown in Fig. 4a [35]. Comparing with pure g-C_3N_4, the Co@g-C_3N_4-1 exhibits approximately the same absorption behavior in the full spectrum, indicating that the 2D conjugated backbone frameworks of g-C_3N_4 are unchanged even after anchoring single-site Co atoms.

Besides, the UV–vis absorption band edges of Co@g-C_3N_4 show an evident redshift phenomenon with increasing the modification density of Co (Fig. S8), which designates an increased π-electron delocalization after incorporation of cobalt. The bandgap energy for Co@g-C_3N_4-1 was estimated to be 2.78 eV, comparable to that of pure g-C_3N_4. The derived flat-band potentials of g-C_3N_4 and Co@g-C_3N_4-1 analyzed from the Mott-Schottky in Fig. 4b were determined to be −0.83 V and −0.95 V vs. the saturated calomel electrode (SCE), respectively. Thus combining the UV–vis results and Mott-Schottky analysis, the corresponding energy levels of the conduction band (CB) and valence band (VB) of these two photocatalysts were illustrated in Fig. 4c. The calculated CB energy levels of Co@g-C_3N_4-1 was more negative with respect to pure g-C_3N_4, and both of which are capable of driving both the photocatalytic hydrogen evolution reaction from splitting water (H^+/H_2: −0.66 V vs SCE at pH 7) and the photocatalytic nitrogen fixation reaction from N_2 (N_2/NH_4^+: −0.57 V vs SCE at pH 7) in thermodynamical. The negative shift in the LUMO energy level of Co@g-C_3N_4-1 indicates a strengthened reducing capability of the photogenerated electrons which will be discussed below [36].

The combined advantages of large surface areas, probably more catalytically active sites, together with suitable band structures and optical properties, make Co@g-C_3N_4 as a promising multifunctional photocatalyst. For verifying this point, the Co@g-C_3N_4 catalysts in different cobalt contents were first employed to drive the photocatalytic hydrogen evolution reaction. The atomic ratio of cobalt in the photocatalyst was determined by the inductively coupled plasma atomic emission spectrometry (ICP-ACE, Shimazu ICP-7510), which shows 0.268, 0.305 and 0.597 wt% for the Co@g-C_3N_4-0.5, Co@g-C_3N_4-1 and Co@g-C_3N_4-2 nanocomposites, respectively. Fig. 4d shows the typical photocatalytic hydrogen production activities of pure g-C_3N_4 and Co@g-C_3N_4 under visible-light illumination, recorded in the water/triethanolamine (TEOA) solution with platinum serving as co-catalyst. As expected, all the samples prepared by our supramolecular methods showed obviously enhanced hydrogen evolution rates alongside the bulk g-C_3N_4, demonstrating that the ordered precursor could result in the optimization of the electronic/band structures in the final g-C_3N_4-based catalysts. Importantly, the introduction of single-site cobalt atoms further strengthens the corresponding photocatalytic activities, especially for the Co@g-C_3N_4-1. It is found that the Co@g-C_3N_4-1 exhibited the optimal activity toward photocatalytic hydrogen production (124 μmol h^{-1}), which gives a 3-fold enhancement of pure g-C_3N_4 (40 μmol h^{-1}), 13-fold of bulk g-C_3N_4 (9 μmol h^{-1}) and is also more competitive than those fo recent state-of-the-art g-C_3N_4-based photocatalysts, including ultrathin g-C_3N_4 nanosheets [37], g-C_3N_4 with intrinsic defect [38], holey g-C_3N_4 nanotubes [39], 17*m*TCPP-CN [40], CdS/WS_2/g-C_3N_4 [41], Mesoporous g-C_3N_4 comprising hollow nanospheres [42], g-C_3N_4 nanosheets/TiO_2 [43], Porous Si-loaded g-C_3N_4 [44], g-C_3N_4/Co@NC [45], Fe@g-C_3N_4 [46], Fe_3C@C/g-C_3N_4 [47], Ni/CM-C_3N_4 [48], P@P-doped g-C_3N_4 [49], 1T-WS_2/2D-g-C_3N_4 [50], g-C_3N_4/C_{60} [51], CdS/MoO_x [23], Cu-TiO_2@C-2% [52] and so on. (Table 1) This could be attributed to the acceleration of the surface reaction kinetics beneficial from the rapid interfacial transportation of the photogenerated electron-hole pairs. Afterward, we also considered the pure catalytic performance of the Co@g-C_3N_4-1, without the deposition of Pt species. As displayed in Fig. S9, the Co@g-C_3N_4-1 shows a photocatalytic H_2 evolution activity of 5.1 μmol h^{-1}, while the pure g-C_3N_4 demonstrates a negligible activity. This phenomenon is limited by the large overpotentials of H_2 production on Co@g-C_3N_4-1 and g-C_3N_4, in keeping with the reported g-C_3N_4-based photocatalysts taking transition metal as cocatalysts [41,47,48].

Long-term stability is another important index to evaluate the photocatalytic hydrogen production performance. Fig. 4e shows the cycling test of continuous hydrogen evolution on the Co@g-C_3N_4-1 photocatalyst for overall 16 h, and every 4 h conducts an intermittent degassing. A total amount of 1.9 mmol H_2 is produced and notably, no evident deterioration of the activities can be observed. The morphologies and structures of the Co@g-C_3N_4-1 photocatalyst after cycling test were also investigated. Fig. S10 shows the typical SEM image of Co@g-C_3N_4-1 after cycling, which demonstrates a porous crimped morphology without degradation and corrosion. FT-IR spectra of Co@g-C_3N_4-1 after cycling exhibits both the typical breathing vibrations of tri-s-triazine units at 810 cm^{-1} and stretching modes of CN heterocycles in the range of 1000–2000 cm^{-1} (Fig. S11), confirming that the intrinsic structures of Co@g-C_3N_4-1 remained. Furthermore, the chemical states of the Co@g-C_3N_4-1 photocatalysts after cycling test were identified by the XPS analysis, shown in Fig. S12. The survey scan spectrum discloses the coexistence of C, N, Co, O, and Pt elements without any other obvious impurity. It should be noted that the Pt species is photodeposited on Co@g-C_3N_4-1 during the visible light irradiation. The chemical states of the Co@g-C_3N_4-1 after cycling test were also in accordance with that of before test, demonstrating reliable stability and an outstanding anti-photocorrosion ability for our novel Co@g-C_3N_4-1 photocatalyst.

Fig. 4f gives the wavelength dependence of the apparent quantum efficiency (AQE) values for hydrogen evolution of the Co@g-C_3N_4-1 catalyst, which illustrates a coincident variation tendency with the above UV–vis absorbance spectra. The Co@g-C_3N_4-1 catalyst displays sharply elevated AQE values during the range of 400–450 nm, especially, the maximum AQE is collected at 420 nm that is ~5.04%, much higher than that of g-C_3N_4 (1.23%). The significantly enhanced photocatalytic hydrogen evolution performance of Co@g-C_3N_4-1 should be attributed to the well-organization of their final structures, and importantly the modification of the single-site cobalt, which greatly optimizes their electronic structures and facilitates the interfacial charge carrier's separation and transportation.

To further elucidate the improvement in photocatalytic via cobalt modification on g-C_3N_4, nitrogen photofixation was also performed in methanol/H_2O solutions under nitrogen bubbling with visible-light illumination. As revealed in Fig. 5a, the bulk g-C_3N_4 shows an extremely low and negligible nitrogen photofixation activity of 8.2 μmol h^{-1}, while for the g-C_3N_4 obtained by our supramolecular method it exhibits a remarkably enhanced activity of 19.5 μmol h^{-1}. After the incorporation of cobalt, it is recognized that the Co@g-C_3N_4-1 is able to achieve an optimal activity as high as 50.2 μmol h^{-1}. In order to confirm the photoproduct NH_4^+ in this reaction system is from N_2 gas, we did the contrast experiment. In the contrast experiment, the photocatalytic nitrogen fixation on Co@g-C_3N_4-1 was carried out under visible light irradiation and a continuous purge with high purity Ar. As shown in Fig. S13, no NH_4^+ was generated within 8 h of visible light irradiation. However, after N_2 being purged, the Co@g-C_3N_4-1 immediately shows the significant photocatalytic nitrogen fixation performance, suggesting that N_2 gas is the N source of NH_4^+. In addition, the concentration of hydrazine hydrate and nitrate species have been estimated during the photocatalytic nitrogen fixation process and the results were shown in Fig. S14. Almost no hydrazine hydrate and nitrate species exit in the final photocatalytic products, indicating that the nitrogen gas involved in the reaction have been eventually converted to ammonium ions.

After that, the nitrogen photofixation activity of the Co@g-C_3N_4-1 discloses no obvious deterioration even after three cycles, demonstrating exceptional stability toward harsh nitrogen photofixation conditions under visible-light illumination (Fig. 5b). It should be noted here that both the hydrogen evolution and nitrogen reduction reaction was consuming and competing for the photogenerated electrons. However, the Co@g-C_3N_4-1 shows negligible photocatalytic hydrogen production performance without the cocatalyst of Pt, as above-mentioned in Fig. S9. It also can be seen that the nitrogen gases involved in the reaction were almost converted into ammonium ions, and no other by-products were generated. Therefore, the Co@g-C_3N_4-1 possesses a relatively high reaction selectivity to ammonia. A possible mechanism for photocatalytic nitrogen fixation on the Co@g-C_3N_4 can be proposed.

Table 1
A summary of recent studies on photocatalytic H_2 production of g-C_3N_4-based materials.

Photocatalyst	Light Source	Co-catalyst	H_2 production rate ($\mu molh^{-1}g^{-1}$)	Ref
Co@g-C_3N_4	300 W Xe lamp (> 420 nm)	3 wt% Pt	2481	this work
Ultrathin g-C_3N_4 nanosheets	300 W Xe lamp (> 420 nm)	3 wt% Pt	570.01	[37]
g-C_3N_4 with intrinsic defect	300 W Xe lamp (> 400 nm)	3 wt% Pt	1469	[38]
Holey g-C_3N_4 nanotubes	300 W Xe lamp (> 420 nm)	0.5 wt% Pt	1073.6	[39]
17*m*TCPP-CN	300 W Xe lamp (> 400 nm)	~12 wt% Pt	2240	[40]
CdS/WS_2/g-C_3N_4	300 W Xe lamp (> 420 nm)	–	1174.5	[41]
Mesoporous g-C_3N_4 comprising hollow nanospheres	300 W Xe lamp (> 420 nm)	3 wt% Pt	659.8	[42]
g-C_3N_4 nanosheets/TiO_2	300 W Xe lamp (> 420 nm)	3 wt% Pt	800	[43]
Porous Si-loaded g-C_3N_4	300 W Xe lamp (> 400 nm)	3 wt% Pt	870.5	[44]
g-C_3N_4/Co@NC	300 W Xe lamp (> 400 nm)	4 wt% Co@NC	1567	[45]
Fe@g-C_3N_4	300 W Xe lamp (> 420 nm)	3 wt% Pt	3390	[46]
Fe_3C@C/g-C_3N_4	300 W Xe lamp (with a filter)	–	272	[47]
Ni/CM-C_3N_4	500 W Xe lamp	10 wt% Ni	313.2	[48]
P@P-doped g-C_3N_4	300 W Xe lamp (> 420 nm)	1 wt% Pt	941.8	[49]
1T-WS_2/2D-g-C_3N_4	300 W Xe lamp (> 420 nm)	64.1% 1 T-WS_2	331.09	[50]
g-C_3N_4/C_{60}	300 W Xe lamp (> 420 nm)	–	266	[51]
CdS/MoO_x	300 W Xe lamp (> 420 nm)	–	2868	[23]
Cu-TiO_2@C-2%	300 W Xe lamp	–	26,910	[52]

$$g\text{-}C_3N_4 + h\nu \rightarrow g\text{-}C_3N_4\ (h^+ + e^-) \quad (1)$$

$$g\text{-}C_3N_4\ (e^-) + Co \rightarrow Co\ (e^-) \quad (2)$$

$$N_2 + 6e^- + 6H^+ \rightarrow 2NH_3 \quad (3)$$

$$NH_3 + H_2O \rightarrow NH_4^+ + OH^- \quad (4)$$

Under the visible-light irradiation, the electron-hole pairs are generated on the surface of g-C_3N_4 (reaction (1)). Simultaneously, the photogenerated electrons can transfer to Co instantly (reaction (2)), resulting in effective charge separation. Consequently, the trapped electrons react with the activated nitrogen to produce ammonia (reaction (3)), which further interact with water to form ammonium ions (reaction (4))

This prominent activity of Co@g-C_3N_4-1 originates mainly from its unique structural features as well as synergistic effects. First, the incorporation of cobalt atoms enhances the specific surface areas of the materials, which significantly strengthens the photocatalytic activities by increasing the population of the triple-phase boundaries in the catalytic system. Further to distinguish the effect of single cobalt atom modification definitely, we normalized the photocatalytic hydrogen evolution rate with surface area and the results were listed in Table S3. It can be clearly seen that the Co@g-C_3N_4-1 process the highest hydrogen production ability of 1.89 and nitrogen fixation performance of

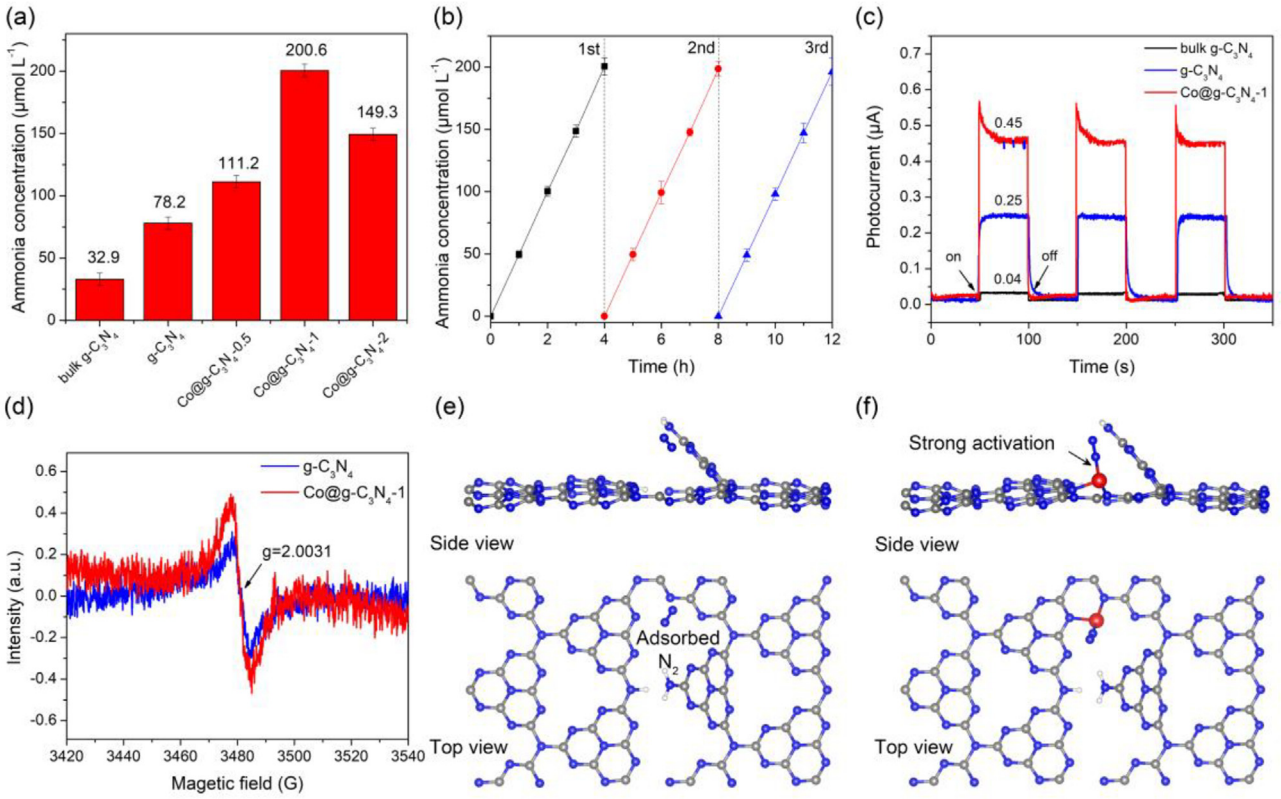

Fig. 5. (a) Yield of NH_3 for different samples under visible light illumination after 4 h, (b) Cycling measurements for photocatalytic nitrogen fixation over Co@g-C_3N_4-1 nanosheets under visible light illumination, (c) Photoelectrochemical responses of bulk g-C_3N_4, g-C_3N_4, and Co@g-C_3N_4-1 under visible light irradiation, (d) EPR spectra of pure g-C_3N_4 and Co@g-C_3N_4-1, (e) N_2 adsorption geometry on pure g-C_3N_4, (f) N_2 adsorption geometry on Co@g-C_3N_4-1.

3.05, compared with that of bulk g-C_3N_4 and pure g-C_3N_4. This phenomenon reveals that the accessible catalytically active sites have been remarkably enhanced after introducing single cobalt atoms, which is extremely beneficial for strengthening the feasibility of H_2 and N_2 activation. After that, DFT computation has been performed to identify the catalytically active sites theoretically. As shown in Fig. 5e, weak adsorption of N_2 on pure g-C_3N_4 can be noticed, which makes it necessary to process further activation. Interestingly, after incorporating the cobalt, the coordinated metal site significantly becomes into the active center with a strong adsorption energy of 0.99 eV (Fig. 5f, Table S4), profiting from that the d-orbital electrons in cobalt atoms are capable of donating to the π N-N antibonding, which potentially realizes the activation of the triple bond of N≡N.[53–59] The N_2 activation process is generally considered as one of the key points in the nitrogen fixation reaction, that is, the Co@g-C_3N_4-1 exhibits enough accessible, highly active catalytically reaction sites, directly acting on their extraordinary catalytic performance.

Second, the optimized band structures of Co@g-C_3N_4-1 catalysts promote the typical behaviours of trapping, migration, and transfer of the excited charge carriers, simultaneously suppresses their radiative recombination. Evidence of that was first given by room-temperature photoluminescence (PL) spectra shown in Fig. S15, it is found the main emission peak of Co@g-C_3N_4-1 was located at 455 nm, which shows an obviously blue-shift by 5 nm in contrast with pure g-C_3N_4. The PL intensities for Co@g-C_3N_4-1 drastically decreased half to that of pure g-C_3N_4, implying the energetically unfavorable charge recombination is substantially inhibited, hence enhancing the charge separation efficiency. Then, electron paramagnetic resonance (EPR) could provide further evidence to this point. As shown in Fig. 5d, slightly boosted EPR signals at g = 2.0031 can be observed in Co@g-C_3N_4-1, which attributes to the unpaired electrons from sp^2-hybridized carbon in the aromatic rings [55]. The introduction of cobalt atoms acts as the bridging sites and redistributes the electrons to the neighboring nitrogen atoms through the delocalized π-conjugated networks in the intrinsic structure of polymeric g-C_3N_4.

Third, a rapid interfacial charge-transport process in Co@g-C_3N_4-1 not only provides an instant transient light response but also generates a high transfer efficiency of the photogenerated charge carriers. Fig. 5c compares the transient photocurrent responses for pure g-C_3N_4 and Co@g-C_3N_4-1 catalysts, which disclosed that both of the catalysts show sensitive responses during on/off cycles upon visible-light illumination. An elevated photocurrent for Co@g-C_3N_4-1 manifests an unsurpassed light response and an efficient photoexcited charge separation with respect to the pure g-C_3N_4. This result was also illustrated by the analysis of electrochemical impedance spectroscopy (EIS) in Fig. S16. In contrast to pure g-C_3N_4, a smaller arc radius for Co@g-C_3N_4-1 indicates that the photoexcited electrons stored in the conduction band can be easily transferred to the protons in the electrolyte [60]. Such a phenomenon could, in turn, promote the separation of photoexcited charge carriers and therefore improve the corresponding photocatalytic performance.

3. Conclusions

In summary, a molecular-level strategy was developed to anchoring and stabilizing single-site cobalt on the porous crimped graphitic carbon nitride, that the final composite is proposed as a photocatalyst to drive solar-photon-driven hydrogen production and nitrogen fixation under ambient conditions. The correlation of experimental results and computational analysis confirms that an optimized electronic structures of the cobalt atom embedded carbon nitride with an appropriate *d*-band position can be achieved. The as-obtained Co@g-C_3N_4 exhibits exceptional photocatalytic hydrogen production rate (2481 μmol h^{-1} g^{-1}, λ > 420 nm) and conspicuous nitrogen photofixation under visible-light irradiation. Such concerted catalysis attributes to the negative shift of the Fermi level in the Co@g-C_3N_4 system deriving from the induced charge-transfer effect, which effectively gains the reducibility of electrons and creates more active sites for photocatalytic reactions.

Declaration of Competing Interest

The authors declare that they have no known competing financial interests or personal relationships that could have appeared to influence the work reported in this paper.

Acknowledgements

This work was supported by National Natural Science Foundation of China (Grant Nos. 51772156 and 51872144), Natural Science Foundation of Jiangsu Province (Grant Nos. BK20180019 and BK20171423), the Fundamental Research Funds for the Central Universities (No. 30917015102, No. 30918014103), PAPD of Jiangsu, the Natural Sciences and Engineering Research Council of Canada (NSERC) and the Ontario government for the Ontario Early Research Award Program.

Appendix A. Supplementary data

Supplementary data to this article can be found online at https://doi.org/10.1016/j.cej.2020.124822.

References

[1] E. Bequerel, Recherches sur les effets de la radiation chimique de la lumière solaire, au moyen des courants électriques, CR Acad. Sci. 9 (1839) 1.
[2] J. Li, H. Li, G. Zhan, L. Zhang, Solar water splitting and nitrogen fixation with layered bismuth oxyhalides, Acc. Chem. Res. 50 (2016) 112–121.
[3] X. Wang, K. Maeda, A. Thomas, K. Takanabe, G. Xin, J.M. Carlsson, K. Domen, M. Antonietti, A metal-free polymeric photocatalyst for hydrogen production from water under visible light, Nature Mater. 8 (2009) 76–80.
[4] G. Zhang, L. Lin, G. Li, Y. Zhang, A. Savateev, X. Wang, M. Antonietti, Ionothermal synthesis of triazine-heptazine based co-frameworks with apparent quantum yields of 60% at 420 nm for solar hydrogen production from“ Sea Water”, Angew. Chem. Int. Ed. 57 (2018) 9372–9376.
[5] M. Shalom, M. Guttentag, C. Fettkenhauer, S. Inal, D. Neher, A. Llobet, M. Antonietti, In situ formation of heterojunctions in modified graphitic carbon nitride: synthesis and noble metal free photocatalysis, Chem. Mater. 26 (2014) 5812–5818.
[6] Y. Fu, T. Huang, L. Zhang, J. Zhu, X. Wang, Ag/g-C_3N_4 catalyst with superior catalytic performance for the degradation of dyes: a borohydride-generated superoxide radical approach, Nanoscale 7 (2015) 13723–13733.
[7] H. Ou, L. Lin, Y. Zheng, P. Yang, Y. Fang, X. Wang, Tri-s-triazine-based crystalline carbon nitride nanosheets for an improved hydrogen evolution, Adv. Mater. 29 (2017) 1700008.
[8] S. Yang, Y. Gong, J. Zhang, L. Zhan, L. Ma, Z. Fang, R. Vajtai, X. Wang, P.M. Ajayan, Exfoliated graphitic carbon nitride nanosheets as efficient catalysts for hydrogen evolution under visible light, Adv. Mater. 25 (2013) 2452–2456.
[9] Y. Zheng, Y. Jiao, J. Chen, J. Liu, J. Liang, A. Du, W. Zhang, Z. Zhu, S.C. Smith, M. Jaroniec, G.Q. Lu, S.Z. Qiao, Nanoporous graphitic-C3N4@carbon metal-free electrocatalysts for highly efficient oxygen reduction, J. Am. Chem. Soc. 133 (2011) 20116–20119.
[10] M. Ledendecker, G. Clavel, M. Antonietti, M. Shalom, Highly porous materials as tunable electrocatalysts for the hydrogen and oxygen evolution reaction, Adv. Funct. Mater. 25 (2015) 393–399.
[11] M. Groenewolt, M. Antonietti, Synthesis of g-C3N4 nanoparticles in mesoporous silica host matrices, Adv. Mater. 17 (2005) 1789–1792.
[12] H. Zhang, G. Liu, L. Shi, H. Liu, T. Wang, J. Ye, Engineering coordination polymers for photocatalysis, Nano Energy 22 (2016) 149–168.
[13] T.Y. Ma, J. Ran, S. Dai, M. Jaroniec, S.Z. Qiao, Phosphorus-doped graphitic carbon nitrides grown in situ on carbon-fiber paper: flexible and reversible oxygen electrodes, Angew. Chem. Int. Ed. 54 (2015) 4646–4650.
[14] S. Yan, Z. Li, Z. Zou, Photodegradation of rhodamine B and methyl orange over boron-doped g-C3N4 under visible light irradiation, Langmuir 26 (2010) 3894–3901.
[15] K. Wang, Q. Li, B. Liu, B. Cheng, W. Ho, J. Yu, Sulfur-doped g-C3N4 with enhanced photocatalytic CO2-reduction performance, Appl. Catal. B: Environ. 176 (2015) 44–52.
[16] J. Fu, B. Zhu, C. Jiang, B. Cheng, W. You, J. Yu, Hierarchical porous O-doped g-C3N4 with enhanced photocatalytic CO2 reduction activity, Small 13 (2017) 1603938.
[17] G. Xu, H. Zhang, J. Wei, H.-X. Zhang, X. Wu, Y. Li, C. Li, J. Zhang, J. Ye, Integrating the g-C3N4 nanosheet with B-H bonding decorated metal-organic framework for CO2 activation and photoreduction, ACS Nano 12 (2018) 5333–5340.

[18] M. Shalom, S. Inal, C. Fettkenhauer, D. Neher, M. Antonietti, Improving carbon nitride photocatalysis by supramolecular preorganization of monomers, J. Am. Chem. Soc. 135 (2013) 7118–7121.

[19] Z. Mo, H. Xu, Z. Chen, X. She, Y. Song, J. Wu, P. Yan, L. Xu, Y. Lei, S. Yuan, Self-assembled synthesis of defect-engineered graphitic carbon nitride nanotubes for efficient conversion of solar energy, Appl. Catal. B: Environ. 225 (2018) 154–161.

[20] Z. Chen, E. Vorobyeva, S. Mitchell, E. Fako, M.A. Ortuño, N. López, S.M. Collins, P.A. Midgley, S. Richard, G. Vilé, A heterogeneous single-atom palladium catalyst surpassing homogeneous systems for Suzuki coupling, Nature Nanotech. 13 (2018) 702–707.

[21] W. Zhang, J. Albero, L. Xi, K.M. Lange, H. Garcia, X. Wang, M. Shalom, One-pot synthesis of nickel-modified carbon nitride layers toward efficient photoelectrochemical cells, ACS Appl. Mater. Interfaces 9 (2017) 32667–32677.

[22] Z. Li, C. Kong, G. Lu, Visible photocatalytic water splitting and photocatalytic two-electron oxygen formation over Cu-and Fe-doped g-C3N4, J. Phys. Chem. C 120 (2015) 56–63.

[23] H. Zhang, P. Zhang, M. Qiu, J. Dong, Y. Zhang, X.W. Lou, Ultrasmall MoOx clusters as a novel cocatalyst for photocatalytic hydrogen evolution, Adv. Mater. 31 (2019) 1804883.

[24] X. Wu, H. Zhang, J. Dong, M. Qiu, J. Kong, Y. Zhang, Y. Li, G. Xu, J. Zhang, J. Ye, Surface step decoration of isolated atom as electron pumping: atomic-level insights into visible-light hydrogen evolution, Nano Energy 45 (2018) 109–117.

[25] H. Zhang, G. Liu, L. Shi, J. Ye, Single-atom catalysts: emerging multifunctional materials in heterogeneous catalysis, Adv. Energy Mater. 8 (2018) 1701343.

[26] W. Zhang, Y. Fu, W. Liu, L. Lim, X. Wang, A. Yu, A General approach for fabricating 3D MFe_2O_4 (M= Mn, Ni, Cu, Co)/graphitic carbon nitride covalently functionalized nitrogen-doped graphene nanocomposites as advanced anodes for lithium-ion batteries, Nano Energy 57 (2019) 48–56.

[27] Z. Chen, S. Pronkin, T.-P. Fellinger, K. Kailasam, G. Vilé, D. Albani, F. Krumeich, R. Leary, J. Barnard, J.M. Thomas, Merging single-atom-dispersed silver and carbon nitride to a joint electronic system via copolymerization with silver tricyanomethanide, ACS Nano 10 (2016) 3166–3175.

[28] H. Zhang, W. Zhou, T. Chen, B.Y. Guan, Z. Li, X.W.D. Lou, A modular strategy for decorating isolated cobalt atoms into multichannel carbon matrix for electrocatalytic oxygen reduction, Energy Environ. Sci. 11 (2018) 1980–1984.

[29] J. Xu, S. Cao, T. Brenner, X. Yang, J. Yu, M. Antonietti, M. Shalom, Supramolecular chemistry in molten sulfur: preorganization effects leading to marked enhancement of carbon nitride photoelectrochemistry, Adv. Funct. Mater. 25 (2015) 6265–6271.

[30] Q. Yao, Y. Liu, R. Lu, C. Xiao, K. Deng, E. Kan, Will a graphitic-like ZnO single-layer be an ideal substrate for graphene? RSC Adv. 4 (2014) 17478–17482.

[31] S. Lany, A. Zunger, Assessment of correction methods for the band-gap problem and for finite-size effects in supercell defect calculations: case studies for ZnO and GaAs, Phys. Rev. B 78 (2008) 235104.

[32] X.X. Wang, D.A. Cullen, Y.T. Pan, S. Hwang, M. Wang, Z. Feng, J. Wang, M.H. Engelhard, H. Zhang, Y. He, Nitrogen-coordinated single cobalt atom catalysts for oxygen reduction in proton exchange membrane fuel cells, Adv. Mater. 30 (2018) 1706758.

[33] Z. Du, X. Chen, W. Hu, C. Chuang, S. Xie, A. Hu, W. Yan, X. Kong, X. Wu, H. Ji, Cobalt in nitrogen-doped graphene as single-atom catalyst for high-sulfur content lithium–sulfur batteries, J. Am. Chem. Soc. 141 (2019) 3977–3985.

[34] Y. Pan, R. Lin, Y. Chen, S. Liu, W. Zhu, X. Cao, W. Chen, K. Wu, W.-C. Cheong, Y. Wang, Design of single-atom Co–N5 catalytic site: a robust electrocatalyst for CO2 reduction with nearly 100% CO selectivity and remarkable stability, J. Am. Chem. Soc. 140 (2018) 4218–4221.

[35] G. Zhang, M. Zhang, X. Ye, X. Qiu, S. Lin, X. Wang, Iodine modified carbon nitride semiconductors as visible light photocatalysts for hydrogen evolution, Adv. Mater. 26 (2014) 805–809.

[36] H. Yu, R. Shi, Y. Zhao, T. Bian, Y. Zhao, C. Zhou, G.I. Waterhouse, L.Z. Wu, C.H. Tung, T. Zhang, Alkali-assisted synthesis of nitrogen deficient graphitic carbon nitride with tunable band Structures for efficient visible-light-driven hydrogen evolution, Adv. Mater. 29 (2017) 1605148.

[37] M.Z. Rahman, J. Ran, Y. Tang, M. Jaroniec, S.Z. Qiao, Surface activated carbon nitride nanosheets with optimized electro-optical properties for highly efficient photocatalytic hydrogen production, J. Mater. Chem. A 4 (2016) 2445–2452.

[38] Z. Zhang, Y. Zhang, L. Lu, Y. Si, S. Zhang, Y. Chen, K. Dai, P. Duan, L. Duan, J. Liu, Graphitic carbon nitride nanosheet for photocatalytic hydrogen production: the impact of morphology and element composition, Appl. Surf. Sci. 391 (2017) 369–375.

[39] X. Wang, C. Zhou, R. Shi, Q. Liu, G.I. Waterhouse, L. Wu, C.-H. Tung, T. Zhang, Supramolecular precursor strategy for the synthesis of holey graphitic carbon nitride nanotubes with enhanced photocatalytic hydrogen evolution performance, Nano Res. 12 (2019) 2385–2389.

[40] E.S. Da Silva, N.M. Moura, M.G.P. Neves, A. Coutinho, M. Prieto, C.G. Silva, J.L. Faria, Novel hybrids of graphitic carbon nitride sensitized with free-base meso-tetrakis (carboxyphenyl) porphyrins for efficient visible light photocatalytic hydrogen production, Appl. Catal. B: Environ. 221 (2018) 56–69.

[41] Y. Zou, J.W. Shi, D. Ma, Z. Fan, L. Cheng, D. Sun, Z. Wang, C. Niu, WS2/graphitic carbon nitride heterojunction nanosheets decorated with CdS quantum dots for photocatalytic hydrogen production, ChemSusChem 11 (2018) 1187–1197.

[42] J. Zhang, Y. Chen, X. Wang, Two-dimensional covalent carbon nitride nanosheets: synthesis, functionalization, and applications, Energy Environ. Sci. 8 (2015) 3092–3108.

[43] H. Zhang, F. Liu, H. Wu, X. Cao, J. Sun, W. Lei, In situ synthesis of gC 3 N 4/TiO 2 heterostructures with enhanced photocatalytic hydrogen evolution under visible light, RSC Adv. 7 (2017) 40327–40333.

[44] Y. Shi, J. Chen, Z. Mao, B.D. Fahlman, D. Wang, Construction of Z-scheme heterostructure with enhanced photocatalytic H2 evolution for g-C3N4 nanosheets via loading porous silicon, J. Catal. 356 (2017) 22–31.

[45] X. Zhou, Y. Zhu, Q. Gao, S. Zhang, C. Ge, S. Yang, X. Zhong, Y. Fang, Modified graphitic carbon nitride nanosheets for efficient photocatalytic hydrogen evolution, ChemSusChem 12 (2019) 4996–5006.

[46] W. Zhang, Q. Peng, L. Shi, Q. Yao, X. Wang, A. Yu, Z. Chen, Y. Fu, Merging single-atom-dispersed iron and graphitic carbon nitride to a joint electronic system for high-efficiency photocatalytic hydrogen evolution, Small 15 (2019) 1905166.

[47] S. Chen, G. Yang, C. Wang, S. Yang, D. Chen, X. Cai, Y. Li, F. Peng, Y. Fang, S. Zhang, Magnetic Fe3C@ C nanoparticles as a novel cocatalyst for boosting visible-light-driven photocatalytic performance of g-C3N4, Int. J. Hydrogen Energy (2019).

[48] L. Bi, D. Meng, Q. Bu, Y. Lin, D. Wang, T. Xie, Electron acceptor of Ni decorated porous carbon nitride applied in photocatalytic hydrogen production, PCCP 18 (2016) 31534–31541.

[49] J. Feng, D. Zhang, H. Zhou, M. Pi, X. Wang, S. Chen, Coupling P nanostructures with P-doped g-C3N4 as efficient visible light photocatalysts for H2 evolution and RhB degradation, ACS Sustain. Chem. Eng. 6 (2018) 6342–6349.

[50] J. Yi, X. She, Y. Song, M. Mao, K. Xia, Y. Xu, Z. Mo, J. Wu, H. Xu, H. Li, Solvothermal synthesis of metallic 1T-WS2: a supporting co-catalyst on carbon nitride nanosheets toward photocatalytic hydrogen evolution, Chem. Eng. J. 335 (2018) 282–289.

[51] X. Chen, H. Chen, J. Guan, J. Zhen, Z. Sun, P. Du, Y. Lu, S. Yang, A facile mechanochemical route to a covalently bonded graphitic carbon nitride (gC 3 N 4) and fullerene hybrid toward enhanced visible light photocatalytic hydrogen production, Nanoscale 9 (2017) 5615–5623.

[52] S. Chen, X. Li, W. Zhou, S. Zhang, Y. Fang, Carbon-coated Cu-TiO2 nanocomposite with enhanced photostability and photocatalytic activity, Appl. Surf. Sci. 466 (2019) 254–261.

[53] C. Lv, Y. Qian, C. Yan, Y. Ding, Y. Liu, G. Chen, G. Yu, Defect engineering metal-free polymeric carbon nitride electrocatalyst for effective nitrogen fixation under ambient conditions, Angew. Chem. Int. Ed. 57 (2018) 10246–10250.

[54] M.-A. Légaré, G. Bélanger-Chabot, R.D. Dewhurst, E. Welz, I. Krummenacher, B. Engels, H. Braunschweig, Nitrogen fixation and reduction at boron, Science 359 (2018) 896–900.

[55] H.-P. Jia, E.A. Quadrelli, Mechanistic aspects of dinitrogen cleavage and hydrogenation to produce ammonia in catalysis and organometallic chemistry: relevance of metal hydride bonds and dihydrogen, Chem. Soc. Rev. 43 (2014) 547–564.

[56] H. Mou, J. Wang, D. Yu, D. Zhang, W. Chen, Y. Wang, D. Wang, T. Mu, Fabricating amorphous g-C3N4/ZrO2 photocatalysts by one-step pyrolysis for solar-driven ambient ammonia synthesis, ACS Appl. Mater. Interfaces 11 (2019) 44360–44365.

[57] H. Mou, J. Wang, D. Zhang, D. Yu, W. Chen, D. Wang, T. Mu, A one-step deep eutectic solvent assisted synthesis of carbon nitride/metal oxide composites for photocatalytic nitrogen fixation, J. Mater. Chem. A 7 (2019) 5719–5725.

[58] S. Cao, H. Chen, F. Jiang, X. Wang, Nitrogen photofixation by ultrathin amine-functionalized graphitic carbon nitride nanosheets as a gaseous product from thermal polymerization of urea, Appl. Catal. B: Environ. 224 (2018) 222–229.

[59] C. Yao, R. Wang, Z. Wang, H. Lei, X. Dong, C. He, Highly dispersive and stable Fe 3+ active sites on 2D graphitic carbon nitride nanosheets for efficient visible-light photocatalytic nitrogen fixation, J. Mater. Chem. A 7 (2019) 27547–27559.

[60] Y. Fu, T. Huang, B. Jia, J. Zhu, X. Wang, Reduction of nitrophenols to aminophenols under concerted catalysis by Au/gC3N4 contact system, Appl. Catal. B: Environ. 202 (2017) 430–437.